DOI: 10.1002/adem.200980050

An X-ray Spectromicroscopy Study of Albumin Adsorption to Crosslinked Polyethylene Oxide Films**

By *Bonnie O. Leung*, Adam P. Hitchcock, John L. Brash, Andreas Scholl* and *Andrew Doran*

Synchrotron-based X-ray photoemission electron microscopy (X-PEEM) is used to characterize the near surface composition of polyethylene oxide (PEO) combined with 1.5, 5, and 10 wt.-% pentaerythritol triacrylate (PETA) crosslinker. It is found that as the concentration of PETA increases, it becomes the dominant component in the top 10 nm of the film surface. The same surfaces are also exposed to human serum albumin (HSA) and the distributions of the protein relative to PEO and PETA measured with X-PEEM. A positive correlation is found between levels of PETA and HSA at the surface. Above PETA concentrations of 5 wt.-%, HSA adsorption is significant, which suggests high levels of PETA (often used to immobilize PEO by crosslinking) can significantly reduce the non-fouling properties of PEO.

Polyethylene oxide (PEO) is a hydrophilic polymer commonly used in biomedical applications to reduce protein adsorption[1] or improve biocompatibility.[2] The effectiveness of PEO for reducing protein adsorption to surfaces likely arises from its molecular conformation in aqueous solution, with repulsive forces developed at certain separation distances resulting in a steric repulsion effect.[3–7] Furthermore, PEO density, chain length, conformation, lack of charge, and its interactions with water are known to affect protein resistance.[8–11]

Since PEO is soluble in water, techniques such as γ, [12] UV[13,14] and electron irradiation[15] have been employed to crosslink the PEO chains to prevent mass loss upon protein exposure. UV-initiated crosslinking of PEO with pentaerythritol triacrylate (PETA) or other radical crosslinkers[16] is becoming increasingly popular, since PEO can be crosslinked in both solution and solid state.[17,18] The inclusion of PETA to form crosslinked PEO has been used in biomedical applications such as hydrogels[19] and micelles[20] for drug delivery, or to form chemically patterned surfaces for cell studies.[21] However, to our knowledge, the effect of PETA crosslinker on the biocompatibility of PEO-based materials has not been systematically investigated.

In this study, we use synchrotron-based X-ray photoemission electron microscopy (X-PEEM) for surface characterization of thin PEO films containing variable levels of PETA crosslinker. We then investigate the effect of the PETA on the adsorption of human serum albumin (HSA) to these surfaces. Previously, we used X-PEEM to study HSA adsorption to phase segregated polystyrene (PS)–poly(methyl methacrylate) (PMMA)[22–26] or PS–polylactide (PLA)[27] thin films. This study is part of an on-going effort to use X-PEEM and other techniques to obtain detailed information on the interfacial interactions of proteins by measuring the distribution of specific proteins over well-characterized, chemically segregated surfaces at high spatial resolution.

Experimental

Materials and Protein Exposure

PEO (MW = 600 000) and PETA were purchased from Sigma Aldrich and used as received. Human serum albumin (HSA) was purchased from Behringwerke AG, Marburg, Germany, and found to be homogeneous as judged by sodium dodecyl sulphate polyacrylamide gel electrophoresis (SDS-PAGE).

[*] *B. O. Leung, Prof. A. P. Hitchcock*
BIMR, McMaster University
Hamilton, ON, L8S 4M1 (Canada)
E-mail: leungbo@mcmaster.ca
Prof. J. L. Brash
School of Biomedical Engineering, McMaster University
Hamilton, ON, L8S 4M1 (Canada)
Dr. A. Scholl, Dr. A. Doran
Advanced Light Source, Berkeley Lab, Berkeley, CA 94720 (USA)

[**] *This research was supported by the Natural Sciences and Engineering Research Council (NSERC, Canada), AFMNet and the Canada Research Chair programs. X-ray microscopy was carried out using PEEM-2 and STXM532 at the ALS. The ALS is supported by the US Department of Energy under Contract DE-AC03-76SF00098.*

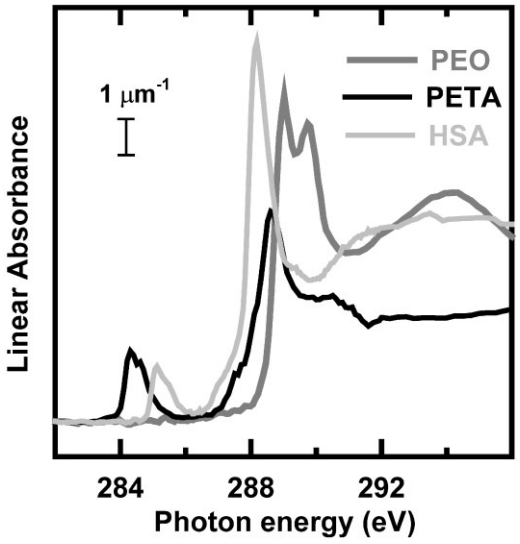

Fig. 1. C 1s X-ray absorption spectra of PEO, PETA and HSA as recorded in STXM. The spectra are plotted on an absolute linear absorbance scale.

To examine the effect of PETA crosslinker, PEO (50 mg) and PETA (0, 1, 5 and 10 wt.-%) were dissolved in dichloromethane (5 g) and spun cast (4 000 rpm, 40 s) onto a clean native oxide silicon wafer. Then the substrates were exposed to a 365 nm UV lamp under flowing nitrogen for 40 min to crosslink the PEO. The films were 100–200 nm thick. Next, the thin films were immersed in 5 mL of 0.005 mg mL^{-1} HSA for 20 min, washed vigorously and air dried. For the PEO sample with 0% PETA, the PEO dissolved upon exposure to protein solution.

X-ray Spectromicroscopy

High quality near-edge X-ray absorption fine structure (NEXAFS) reference spectra of PEO, PETA and HSA (Figure 1) were collected with the scanning transmission X-ray microscope (STXM) on beamline 5.3.2 at the Advanced Light Source (ALS) in Berkeley, CA [28,29]. While the STXM beamline has better energy resolution (0.1–0.2 eV) compared to the X-PEEM beamline (0.4–0.5 eV), similar spectral lineshapes were obtained from both techniques. Samples for STXM were solvent-cast onto an X-ray transparent silicon nitride window (75 nm thick, 1 mm × 1 mm, Norcada Inc) and micrometer-sized areas were probed using image sequences (stacks) [30]. The intensity scale of each reference spectrum was normalized to the signal expected from 1 nm of the polymer or protein at its bulk density.

X-PEEM data collection was performed at the ALS on beamline 7.3.1 with the PEEM-2 microscope. Briefly, photoelectrons and secondary electrons are ejected upon absorption of 70%–80% left circularly polarized monochromatic X-rays. The electron distribution is magnified with an electrostatic imaging column and the spatial distribution is detected with a CCD camera [31]. X-PEEM is a total electron yield technique that probes the top 10 nm of the sample, with a measured sampling depth of (1/*e*) of 4 nm for organic polymers [32]. A 100 nm thick titanium filter was used to reduce second-order light. A shutter with a 0.1 s response time blocked the X-ray beam except during image acquisition.

X-PEEM Data Analysis

All data analyses were performed with the aXis2000 software package [33]. C 1s image sequences were aligned and then normalized to the ring current and to the I_0 spectrum obtained from a clean HF-etched Si chip. The I_0 spectrum was corrected for the absorption of underlying silicon and the linear bolometric response function of the detector. The energy scales were set by calibrating the C 1s $\rightarrow \pi^*_{C=C}$ transition of a clean polystyrene sample to 285.15 eV.

Singular value decomposition was used to fit the C 1s spectrum at each pixel of an image sequence with the PEO, PETA and HSA reference spectra [34,35]. The fit coefficients obtained from the SVD fit are assembled into component maps, which show the spatial distribution of each component. Non-uniform illumination was compensated by dividing each component map with a heavily smoothed image of the sum of all components. Furthermore the intensity of each image was divided by a scale factor which results in a total average thickness (sum of all components) of 10 nm, the total depth sampled by X-PEEM [25].

PEO-rich and PETA-rich areas were examined quantitatively by applying a threshold mask to the stack to obtain pixels specific to PEO or PETA (Figure 2). Only pixels above a defined value were included and the average NEXAFS spectrum from each masked region was further altered by setting the pre-edge intensity to zero. Each PEO- or PETA-rich average NEXAFS spectrum was then fitted with the PEO, PETA and HSA reference spectra. For each type of sample, several stacks were quantitatively examined and the results were averaged to determine the uncertainty or standard deviation.

Results and Discussion

The C 1s reference spectra for PEO, PETA and HSA are plotted in Figure 1. The three species can be easily distinguished at the C 1s edge. The PEO spectrum is dominated by C 1s $\rightarrow \sigma^*_{C-H}$ and C 1s $\rightarrow \sigma^*_{C-O}$ transitions at 289.0 and 289.8 eV, respectively.[36] PETA is characterized by two main transitions at 284.5 and 288.6 eV, corresponding to C 1s $\rightarrow \pi^*_{C=C}$ and C 1s $\rightarrow \pi^*_{C=O}$ transitions, respectively. The C=C π^* transition at 284.5 eV is 0.7 eV lower than the corresponding C 1s $\rightarrow \pi^*_{C=C}$ transition in PS due to conjugation of double bonds in the PETA structure. HSA shows a strong C 1s $\rightarrow \pi^*_{C=O}$ transition at 288.20 eV, which is 0.4 eV lower than the C 1s $\rightarrow \pi^*_{C=C}$ transition of PETA due to the less electronegative environment of the carbon atom in the amide group of proteins.

The color-coded maps of the PEO films with 1.5, 5 and 10 wt.-% PETA crosslinker obtained from X-PEEM are shown in Figure 3. The same data are presented in two different ways. In the rescaled maps (Fig. 3d, i and n) the intensity of each component is mapped separately to the full range of its color

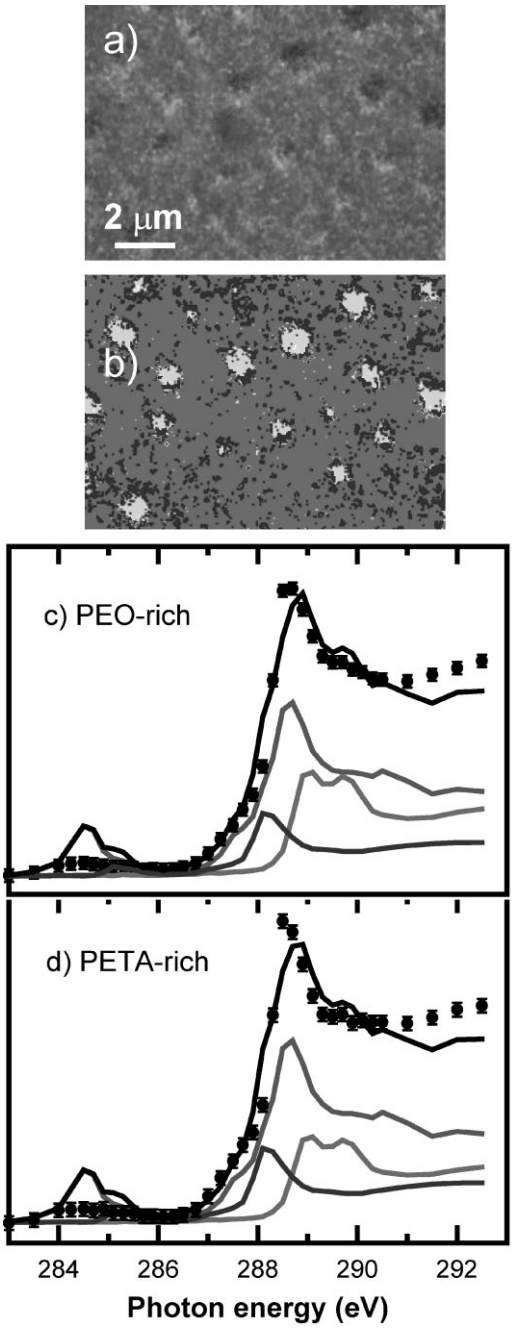

Fig. 2. a) Sample X-PEEM color coded composite map (non-rescaled) derived from a singular value decomposition (SVD) analysis, using the PEO, PETA and HSA reference spectra (Fig. 1), of a C 1s image sequence (23 energies) recorded from a spun-cast PEO blend with 10% PETA contribution. b) Mask used to extract spectra of specific regions. Red denotes PEO-rich regions, green denotes PETA-rich regions, defined by threshold masking the PS and PEO component maps. The remaining blue pixels define areas at the interface between the PEO-rich and PETA-rich domains and were not used in the fitting procedure. c) Curve fit of the average C 1s spectra of the PEO-rich region (data, dots; fit, black line; components, colored lines) d) Curve fit of the average C 1s spectra of the PETA-rich region (same color coding).

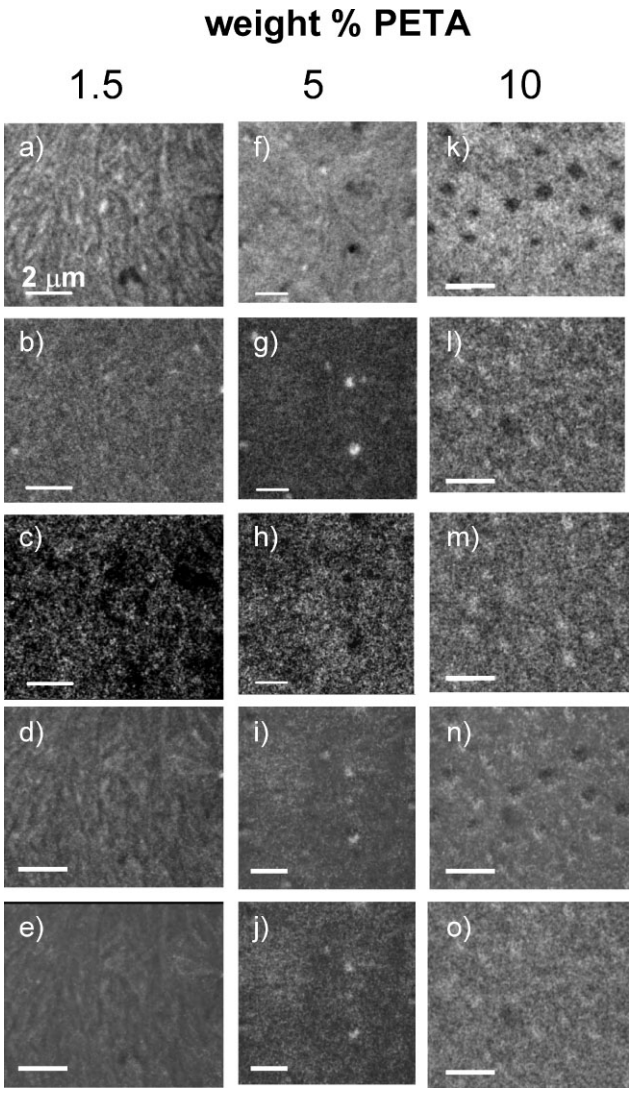

Fig. 3. X-PEEM color coded composite maps of PEO with 1.5% PETA crosslinker: a) PEO, b) PETA, c) HSA, d) rescaled, e) absolute; PEO with 5% PETA: f) PEO, g) PETA, h) HSA, i) rescaled, j) absolute; and, PEO with 10% PETA: k) PEO, l) PETA, m) HSA, n) rescaled, o) absolute. PEO is coded red, PETA is coded green and HSA is coded blue.

(0–255), resulting in greater sensitivity for the localization of each component. In the absolute maps (Fig. 3e, j and o) the intensity of each component is displayed on a common scale (0–10 nm), which preserves the thickness information.

The rescaled color coded image for the 1.5 wt.-% PETA sample (Fig. 3d) reveals an inhomogeneous surface with small PETA domains (of approximately 50 nm) scattered within a PEO matrix, with PEO, PETA and HSA color coded as red, green and blue, respectively. These small PETA domains are hard to resolve and may be beyond the resolution limits of the X-PEEM used for these studies. As the concentration of crosslinker increases, the surface evolves from slightly structured to having large circular domains of green cross-linked PETA. With increasing crosslinker concentration, the images become pinker and teal, indicative of HSA adsorption to the entire surface. At the highest PETA concentration studied (10 wt.-%), there is a marked correlation between the green dots of PETA and intensely blue HSA (Fig. 3n).

The absolute color-coded images show the surface changing from bright red (Fig. 3e) to bright green (Fig. 3o)

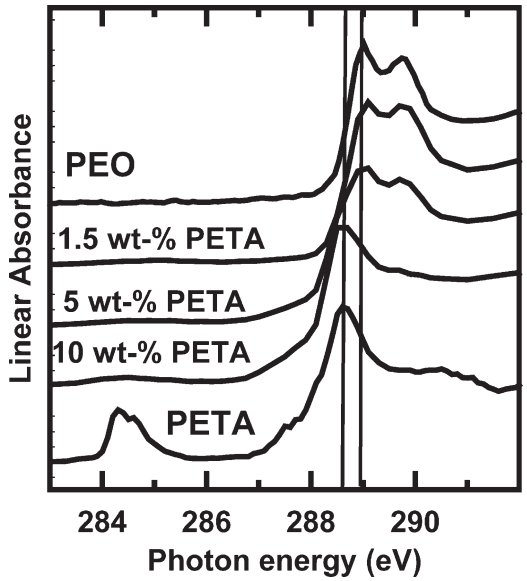

Fig. 4. C 1s X-ray absorption spectra of PEO with 1.5%, 5% and 10% PETA, compared to the spectra of pure PEO and PETA.

as the concentration of PETA increases from 1.5% to 10%, suggesting that surface enrichment of PETA occurs at the substrate–air interface. In these images, the blue color representing HSA is faint indicating that although PETA segregates to the surface, the PEO still retains some protein resistance.

Figure 4 compares the average spectra extracted from the 1.5, 5 and 10 wt.-% PETA samples compared to pure PEO and pure PETA. As the concentration of PETA increases the main NEXAFS peak shifts to lower energy and the spectral line shape changes from mainly PEO (1.5 wt.-% PETA sample) to mainly PETA (10 wt.-% PETA sample).

Doytcheva et al. suggested that under UV irradiation, PETA (singlet) undergoes an intersystem crossing to form an excited triplet state which is capable of cleaving a proton from PEO to form a PEO radical and a PETA radical.[15] Our experiments verify that PETA acts as both an initiator and a crosslinker since UV irradiation of PEO alone does not form crosslinked PEO. Also, our NEXAFS spectra show almost no intensity in the C $1s \rightarrow \pi^*_{C=C}$ transition at 284.5 eV, which should be seen if the double bonds of PETA were still present. This clearly indicates that the crosslinking mechanism occurs by PEO and PETA radical attack of the PETA double bond. FTIR analysis of PEO crosslinked with PETA for micelle formation also showed no evidence of C=C double bonds indicating complete radical polymerization.[37]

The quantitative results extracted from PEO- and PETA-rich areas are summarized in Table 1. For the 1.5 wt.-% PETA sample, a small amount of PETA (0.7 nm) is detected in the PEO-rich area. At this low crosslinker concentration, PEO still retains its non-fouling properties with no detectable HSA adsorption. The PETA-rich area shows an increase of 6% PETA, revealing that PEO remains the dominating component (at approximately 90%) across the top 10 nm of the surface. HSA is not detected, even in the PETA-rich areas.

Table 1. Thickness of PEO, PETA and HSA in PEO- and PETA-rich areas for 1 wt.-% PEO samples with 1.5, 5 and 10 wt.-% PETA concentration. These films were exposed to 0.005 mg mL^{-1} HSA in DDI water. Uncertainty: ±0.5 nm.

Region	Composite thickness [nm]	Amount of PETA [wt.-%]		
		1.5	5	10
PEO	PEO	9.3	5.7	2.2
	PETA	0.7	3.7	6.5
	HSA	*0.0*	*0.7*	*1.3*
PETA	PEO	8.7	4.8	1.6
	PETA	1.3	4.9	7.0
	HSA	*0.0*	*0.3*	*1.4*

However, as the concentration of PETA increases to 5 wt.-%, a detectable amount of HSA adsorbs to the surface. At 5 wt.-% PETA, the crosslinker thickness in the PEO-rich areas increases from 0.7 to 3.7 nm, while in the PETA-rich area, it increases by almost four-fold to 4.9 nm. At this relatively low PETA concentration (5 wt.-%), the top 10 nm of the surface shows a mixture of approximately 50:50 PEO/PETA with 0.3–0.7 nm of HSA. These results show that PETA is strongly surface segregated. Typically, if there is sufficient mobility in polymer systems, the component with the lower surface free energy segregates to the surface.[38] Since PETA is more hydrophobic than PEO,[37] PETA should have lower surface free energy and would be expected to segregate to the surface.[39,40] Furthermore, the molecular weight difference between PETA and PEO should also affect the surface composition with the lower molecular weight PETA segregating to the surface.[41]

At 10 wt.-% PETA, the crosslinker becomes the dominant component (65–70%) at the surface for both the PEO-and PETA-rich regions. Here, the thickness of adsorbed protein doubles to 1.3–1.4 nm across the entire surface with only a small amount of PEO (15–20%) detectable. These quantitative results show that at a crosslinker concentration greater than 5 wt.-%, the PEO surface begins to lose its non-fouling properties and begins to adsorb protein. As the concentration of PETA increases, the amount of adsorbed HSA also increases, suggesting that HSA binds preferentially to the crosslinker. Furthermore, small regions of PETA enrichment in the surface below the spatial resolution of the X-PEEM microscope may also cause irreversible protein adsorption to those regions of the surface.

Recently, fluorescence microscopy treated by integral geometry analysis was used to quantify the adsorption of labeled lentil lectin (LcH) or concavalin A (ConA) to several polymeric surfaces including PEO crosslinked with PETA.[42] While this technique can spatially resolve and quantify lectin adsorption to the surface, it provides no information on the polymeric substrate. This fluorescence study suggested that lectin adsorption may be influenced to some extent by the

presence of PETA; however, since the spun-cast PEO film studied was prepared using 15% PETA, the crosslinker is undoubtedly the dominant component of the film surface.

The inclusion of PETA and other UV-initiated radical crosslinkers[16] to form PEO-based biomaterials such as hydrogels[11,17] or micelles[18] for drug delivery is becoming increasingly common. In the formation of micelles, PETA is used to stabilize the hydrophobic core[26] and is likely not present at the air–substrate interface. However, for hydrogel or micro-array applications, it is likely that the highly surface active PETA crosslinker is present as a major component at the interface, and as such may compromise the antifouling properties of PEO.

Conclusions

PEO containing 1.5, 5 and 10 wt.-% PETA was crosslinked by UV exposure, exposed to 0.005 mg mL^{-1} HSA and examined with X-PEEM. As the concentration of PETA increased, it became the dominant component in the top 10 nm of the surface. Upon exposure to HSA, increased protein adsorption was seen with increasing PETA concentration. It is concluded that at PETA concentrations above 5 wt.-%, PEO begins to lose its non-fouling properties.

Received: November 16, 2009
Final Version: January 4, 2009
Published online: April 7, 2010

[1] E. W. Merrill, K. A. Dennison, C. Sung, *Biomaterials* **1993**, *14*, 1117.
[2] C. P. Quinn, C. P. Patha, A. Heller, J. A. Hubbell, *Biomaterials* **1995**, *16*, 389.
[3] R. Kjellander, E. Florin, *J. Chem. Soc. Faraday Trans 1*, **1981**, *77*, 2023.
[4] J. Andrade, (Ed.), in: *Surface and Interfacial Aspects of Biomedical Polymers*, Plenum, New York **1985**, Ch. 1.
[5] J. Klein, P. Luckham, *Nature* **1982**, *300*, 429.
[6] P. Luckham, J. Klein, *Macromolecules* **1985**, *18*, 721.
[7] S. I. Leon, J. H. Lee, J. D. Andrade, P. G. de Gennes, *J. Colloid Interface Sci.* **1991**, *142*, 149.
[8] L. D. Unsworth, Z. Tun, H. Sheardown, J. L. Brash, *J. Colloid Interface Sci.* **2006**, *296*, 520.
[9] M. Malmsten, K. Emoto, J. M. Van Alstine, *J. Colloid Interface Sci.* **1998**, *202*, 507.
[10] S. Tosatti, S. M. De Paul, A. Askendal, S. Vandevondele, J. A. Hubbell, P. Tengvall, M. Textor, *Biomaterials* **2003**, *24*, 4949.
[11] E. A. Vogler, *J. Biomater. Sci., Polym. Ed.* **1999**, *10*, 1015.
[12] J. L. Stringer, N. A. Peppas, *J. Controlled Release* **1996**, *42*, 195.
[13] M. Doycheva, R. Stamenova, V. Zvetkov, C. B. Tsvetanov, *Polymer* **1998**, *39*, 6715.
[14] M. B. Mellott, K. Searcy, M. V. Pishko, *Biomaterials* **2001**, *22*, 929.
[15] P. Kofinas, V. Athanassiou, E. W. Merrill, *Biomaterials* **1996**, *17*, 1547.
[16] M. Doytcheva, D. Dotcheva, R. Stamenova, A. Orahovats, Ch. Tsvetanov, J. Leder, *J. Appl. Polym. Sci.* **1998**, *64*, 2299.
[17] M. Doycheva, E. Petrova, R. Stamenova, C. Tsvetanov, G. Riess, *Macromol. Mater. Eng.* **2004**, *289*, 676.
[18] M. Doytcheva, D. Dotcheva, R. Stamenova, C. Tsvetanov, *Macromol. Mater. Eng.* **2001**, *286*, 30.
[19] M. Dimitrov, D. Dotcheva, N. Lambov, *Acta Pharm. Turcica* **2004**, *46*, 49.
[20] P. Petrov, M. Bozukov, M. Burkhardt, S. Muthukrishnan, A. H. E. Müller, C. B. Tsvetanov, *J. Mater. Chem.* **2006**, *16*, 2192.
[21] M. C. Lensen, P. Mela, A. Mourran, J. Groll, J. Heuts, H. Rong, M. Möller, *Langmuir* **2007**, *23*, 7841.
[22] C. Morin, A. P. Hitchcock, R. M. Cornelius, J. L. Brash, A. Scholl, A. Doran, *J. Elec. Spec.* **2004**, *137-140*, 785.
[23] L. Li, A. P. Hitchcock, N. Robar, R. M. Cornelius, J. L. Brash, A. Scholl, A. Doran, *J. Phys. Chem. B* **2006**, *110*, 16763.
[24] B. O. Leung, A. P. Hitchcock, R. M. Cornelius, J. L. Brash, A. Scholl, A. Doran, *Biomacromolecules* **2009**, *10*, 1838.
[25] L. Li, A. P. Hitchcock, R. M. Cornelius, J. L. Brash, A. Scholl, A. Doran, *J. Phys. Chem. B* **2008**, *112*, 2150.
[26] B. O. Leung, A. P. Hitchcock, J. L. Brash, A. Scholl, A. Doran, P. Henklein, J. Overhage, K. Hilpert, J. D. Hale, R. E. W. Hancock, *Biointerphases* **2008**, *3*, F27.
[27] B. O. Leung, A. P. Hitchcock, J. L. Brash, A. Scholl, A. Doran, *Macromolecules* **2009**, *42*, 1679.
[28] T. Warwick, H. Ade, A. L. D. Kilcoyne, M. Kritscher, T. Tylisczcak, S. Fakra, A. P. Hitchcock, P. Hitchcock, H. A. Padmore, *J. Synch. Rad.* **2002**, *9*, 254.
[29] A. L. D. Kilcoyne, T. Tylisczak, W. F. Steele, S. Fakra, P. Hitchcock, K. Franck, E. Anderson, B. Harteneck, E. G. Rightor, G. E. Mitchell, A. P. Hitchcock, L. Yang, T. Warwick, H. Ade, *J. Synch. Rad.* **2003**, *10*, 125.
[30] C. J. Jacobsen, C. Zimba, G. Flynn, S. Wirick, *J. Microsc.* **2000**, *19*, 173.
[31] S. Anders, H. A. Padmore, R. M. Duarte, T. Renner, T. Stammler, A. Scholl, M. R. Scheinfein, J. Stohr, L. Seve, B. Sinkovic, *Rev. Sci. Instrum.* **1999**, *70*, 3973.
[32] J. Wang, L. Li, C. Morin, A. P. Hitchcock, A. Doran, A. Scholl, *J. Electron Spectrosc.* **2009**, *170*, 25.
[33] aXis2000 is free for non-commercial use. It is written in Interactive Data Language (IDL) and available from http://unicorn.mcmaster.ca/aXis2000.html.
[34] G. Strang, *Linear Algebra and Its Applications*, Harcourt Bracourt, Jovanovich, San Diego **1988**.
[35] I. N. Koprinarov, A. P. Hitchcock, C. T. McCrory, R. F. Childs, *J. Phys. Chem. B* **2002**, *106*, 5358.
[36] J. Kikuma, B. P. Tonner, *J. Electron Spectrosc. Relat. Phenom.* **1996**, *82*, 53.

[37] P. Petrov, M. Bozukov, C. B. Tsvetanov, *J. Mater. Chem.* **2005**, *15*, 1481.
[38] C. Ton-That, A. G. Shard, D. O. H. Teare, R. H. Bradley, *Polymer* **2001**, *42*, 1121.
[39] S. C. Lim, S. H. Kim, J. H. Lee, M. K. Kim, D. J. Kim, T. Zyung, *Synth. Met.* **2005**, *148*, 75.
[40] T. P. Russel, *Science* **2002**, *297*, 964.
[41] T. F. Schaub, G. J. Kellogg, A. M. Mayes, R. Kulasekere, J. F. Ankner, H. Kaiser, *Macromolecules* **1996**, *29*, 3982.
[42] J. Zemla, M. Lekka, J. Wiltowska-Zuber, A. Budkowski, J. Rysz, J. Raczkowska, *Langmuir* **2008**, *24*, 10243.

